Chapter 2
Computational Techniques for the LHC

Although the search for the Higgs boson is motivated by the electroweak interaction, a detailed knowledge of quantum chromodynamics (QCD) is required to make precise predictions at a hadron collider such as the LHC. However, these calculations are troublesome; QCD describes the interactions of quarks and gluons, though only the composite hadrons are experimentally observed.

Some key concepts of QCD are introduced in Sect. 2.1, before the simulation of LHC collisions is described in Sect. 2.2. Finally, jets are introduced in Sect. 2.3 as useful tools connecting theoretical calculations with experimental observations.

2.1 Quantum Chromodynamics

QCD is the theory of the strong interaction, describing coloured particles (quarks and gluons, collectively known as partons) [1]. Two crucial features of QCD are *confinement* and *asymptotic freedom*. Confinement refers to the observation that quarks and gluons are only found within colourless hadrons, and never as isolated states. Asymptotic freedom states that, within the hadron, the constituent partons are relatively free to move. Both concepts can be understood in terms of a running coupling constant.

2.1.1 Renormalisation and the Running Coupling Constant

When calculating observables within perturbative quantum field theory, ultraviolet (UV) divergences are often introduced by Feynman diagrams containing loops. Through careful consideration, these UV divergences can be absorbed into renormalised definitions of the coupling constant and particle masses. The idea is that the 'bare' quantities contain compensating divergences, such that the physically measurable quantities are finite:

D. Hall, *Discovery and Measurement of the Higgs Boson in the WW Decay Channel*, Springer Theses, DOI 10.1007/978-3-319-19989-4_2

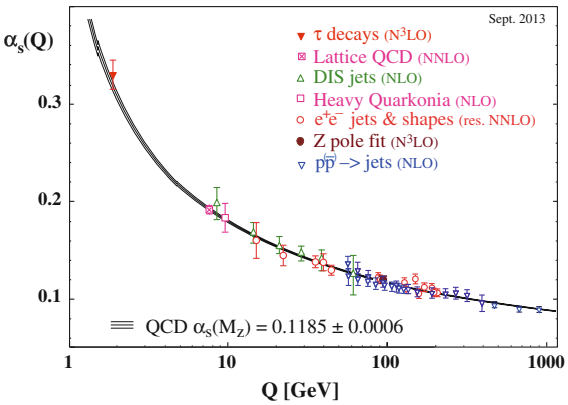

Fig. 2.1 The running of the strong coupling constant α_S with energy scale Q [6]. Experimental measurements at various scales are also shown

$$g_{\text{physical}} = g_{\text{bare}} + \delta g \qquad \text{and} \qquad m_{\text{physical}} = m_{\text{bare}} + \delta m \tag{2.1}$$

where δg and δm are the loop contributions. This procedure is known as *renormalisation*.

It is necessary to introduce an unphysical *renormalisation scale* μ_R, above which loops are absorbed into renormalised quantities, and below which loops are calculated in perturbation theory. The exact details of the separation depend upon the choice of renormalisation scheme [2]. Clearly couplings and masses will depend upon μ_R, though physical observables must not; however, truncation of the perturbative series will result in a residual μ_R dependence. Usually μ_R is chosen to be the energy scale Q of the process under consideration, leading to the concept of a *running coupling constant*.

The QCD coupling constant α_S is shown in Fig. 2.1. At low scales (large distances), α_S is large and the theory is non-perturbative. Though not analytically proven[1], confinement has been verified in this regime by lattice QCD [3]. At high scales (small distances), α_S is small; this is asymptotic freedom [4, 5]. Note that α_{EM} in QED exhibits an opposite trend, though remains perturbative at all accessible energies.

2.1.2 Perturbative QCD

Most interesting LHC processes involve a large momentum transfer, where the partons are asymptotically free. Thus, parton-level cross sections may be calculated with Feynman diagrams as a perturbative series in α_S (which converges since $\alpha_S \ll 1$)

$$\hat{\sigma} = \sum_{m=0}^{\infty} \alpha_S^{k+m} \hat{\sigma}^{(m)} \tag{2.2}$$

[1] A mathematically rigorous proof of confinement is one of seven Millennium Prize Problems of the Clay Mathematics Institute, with a bounty of $1,000,000.

where the hat denotes a parton-level quantity, k is the number of QCD vertices at tree-level, and $\hat{\sigma}^{(m)}$ is the mth order contribution to the cross section. A *fixed order* calculation truncates the series after n terms, with $n = 0$ being a leading order (LO) calculation, $n = 1$ being a next-to-leading order (NLO) calculation, and so on.

As mentioned in Sect. 2.1.1, the cross section $\hat{\sigma}$ is independent of the renormalisation scale μ_R

$$\frac{\mathrm{d}\hat{\sigma}}{\mathrm{d}\mu_R} = 0\,. \tag{2.3}$$

However, real-life calculations always truncate the series after n terms, leaving a residual μ_R dependence. Inserting the truncated series into (2.3), it follows that

$$\frac{\mathrm{d}}{\mathrm{d}\mu_R}\sum_{m=0}^{n}\alpha_S^{k+m}\hat{\sigma}^{(m)} = -\frac{\mathrm{d}}{\mathrm{d}\mu_R}\sum_{m=n+1}^{\infty}\alpha_S^{k+m}\hat{\sigma}^{(m)} \tag{2.4}$$

$$= \mathcal{O}\left(\alpha_S^{k+n+1}\right)\,. \tag{2.5}$$

Thus, the residual μ_R dependence can be exploited to probe the effect of missing higher order terms in the series, and estimate the associated uncertainty.

2.1.3 Resummation of Large Logarithms

Fixed order calculations are useful only when the perturbative series is converging, as is usual for an inclusive cross section. However, when considering exclusive observables, there are regions of phase space in which the missing higher order terms contribute as much as the included terms. This often occurs when there is a large separation in the scales of the exclusive observables and the process.

For example, consider the emission of a gluon from an outgoing quark. The scale separation of the hard scatter Q from the soft emission Q_1 introduces Sudakov double logarithmic contributions $\alpha_S^{k+m}L^{2m}$ to the perturbative series, where $L \sim \ln(Q_1/Q)$. Requiring such an emission, the (schematic) structure of the perturbative series becomes

$$\hat{\sigma} \sim \alpha_S^k\left\{\alpha_S\left(L^2+L+1\right)+\alpha_S^2\left(L^4+L^3+L^2+L+1\right)+\mathcal{O}\left(\alpha_S^3L^6\right)\right\}\,. \tag{2.6}$$

Soft or collinear emissions are defined by $\alpha_S\,L^2 \approx 1$, such that the logarithms overcome the α_S suppression. Thus, the perturbative nature of the series is spoiled. In (2.6), terms like $\alpha_S^{k+m}L^{2m}$ are called leading logarithms (LLs), terms like $\alpha_S^{k+m}L^{2m-1}$ are called next-to-leading logarithms (NLLs), and so on.

When an observable is sensitive to such large logarithms, they must be *resummed* to all orders in α_S to produce an accurate result. This is usually achieved analytically,

but in this example of soft and collinear emissions a *parton shower* Monte Carlo program can be used. This probabilistically generates emissions as it evolves partons from the scale of the hard scatter down to a scale where non-perturbative effects of confinement dominate. This leads to fully-exclusive observables. A parton shower is necessary to produce hadron-level predictions (see Sect. 2.2). Formally they have LL accuracy, though can include many higher order logarithms through the enforcement of physical effects such as energy-momentum conservation and colour coherence.

2.1.4 Parton Distribution Functions

Since confinement binds partons into hadrons, it is the latter that are accelerated and collided at the LHC (in particular protons). Therefore, we need to calculate observables for proton-proton interactions rather than the parton-parton interactions discussed above. Fortunately, the *factorisation theorem* states that the soft non-perturbative physics of the hadron can be treated independently of the hard scatter [7]. Thus, a proton-proton cross section can be formulated as a convolution of the partonic cross section with parton distribution functions (PDFs) of the incoming protons. That is,

$$\sigma(p_1, p_2) = \sum_{a,b} \int_0^1 \mathrm{d}x_1 \mathrm{d}x_2 f_a\left(x_1, \mu_\mathrm{F}^2\right) f_b\left(x_2, \mu_\mathrm{F}^2\right) \widehat{\sigma}_{\mathrm{ab}}\left(x_1 p_1, x_2 p_2, \alpha_\mathrm{S}\left(\mu_\mathrm{R}^2\right), \frac{Q^2}{\mu_\mathrm{F}^2}, \frac{Q^2}{\mu_\mathrm{R}^2}\right) \tag{2.7}$$

where f_a is the PDF of parton type a within the proton, p_i is the momentum of proton i, x_i is the momentum fraction of parton i, and Q is the scale of the hard scatter. A sum is performed over all possible parton types (six quark flavours and the gluon).

Echoing renormalisation, factorisation absorbs collinear divergences into universal PDFs which are not *a priori* calculable and must be experimentally constrained. An unphysical *factorisation scale* μ_F is introduced, below which emissions are absorbed into PDFs, and above which they are included in the hard scatter. As with μ_R, truncating the perturbative series introduces a μ_F dependence, which can be exploited to estimate the effect of the missing higher order terms. At LO, $f_a(x, \mu_\mathrm{F})$ is simply the probability of finding a parton of type a with momentum fraction x, when probing the proton at a scale μ_F. However, the interpretation at higher orders is more complicated.

The PDF μ_F scaling is described by the DGLAP equations [8–10]. Thus, an $f_a(x)$ ansatz is made at low μ_F and then experimentally validated at higher scales (e.g with deep inelastic scattering or collider jet data). Figure 2.2 shows some example PDFs.

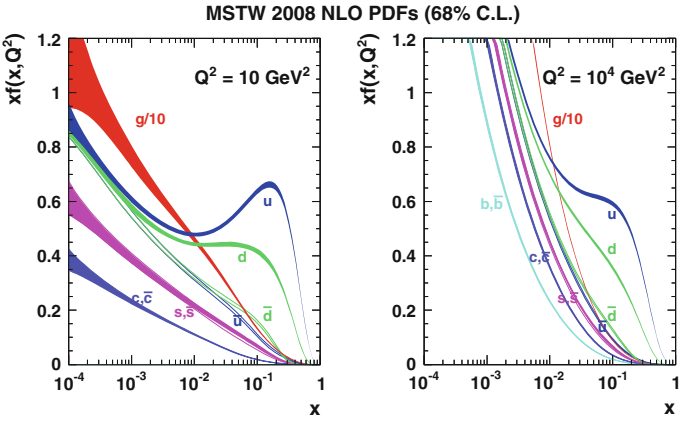

Fig. 2.2 Parton distribution functions fit by the MSTW collaboration, evaluated at $\mu_F^2 = 10\,\text{GeV}^2$ (*left*) and $\mu_F^2 = 10^4\,\text{GeV}^2$ (*right*) [11]. Note that the gluon PDF is suppressed by a factor 10. Reprinted with kind permission from Springer Science and Business Media: European Physical Journal C, **63**, 2009, 189–285, *Parton distributions for the LHC*, A. D. Martin, W. J. Stirling, R. S. Thorne and G. Watt, Fig. 2.1, Copyright 2009. MSTW 2008 NLO PDFs at $Q^2 = 10\,\text{GeV}^2$ and $Q^2 = 10^4\,\text{GeV}^2$

2.2 Monte Carlo Event Generation

Monte Carlo (MC) event generators provide a fully-exclusive hadron-level simulation of pp collision events at the LHC [12]. This section will describe the basic features of a simulated event, before discussing some more advanced techniques that shall be used throughout the thesis.

2.2.1 The Anatomy of an Event

Figure 2.3 shows how the MC event generation is factorised into several components, each describing a certain regime of momentum transfer.

Hard scatter

The high scale process can be selected as desired (e.g Higgs boson production via gluon-gluon fusion). The relevant parton-level matrix elements (MEs) are calculated using fixed order perturbative QCD, either by the event generator itself or an external program. Historically, these MEs were usually LO, though improvements are discussed in Sects. 2.2.3 and 2.2.4.

Parton distribution functions (PDFs)

Incoming parton momenta are sampled from a proton PDF, usually probed at the scale of the hard scatter ($\mu_F = Q$). The LHAPDF interface [14] provides access to the PDFs of several fitting collaborations, such as CTEQ [15],

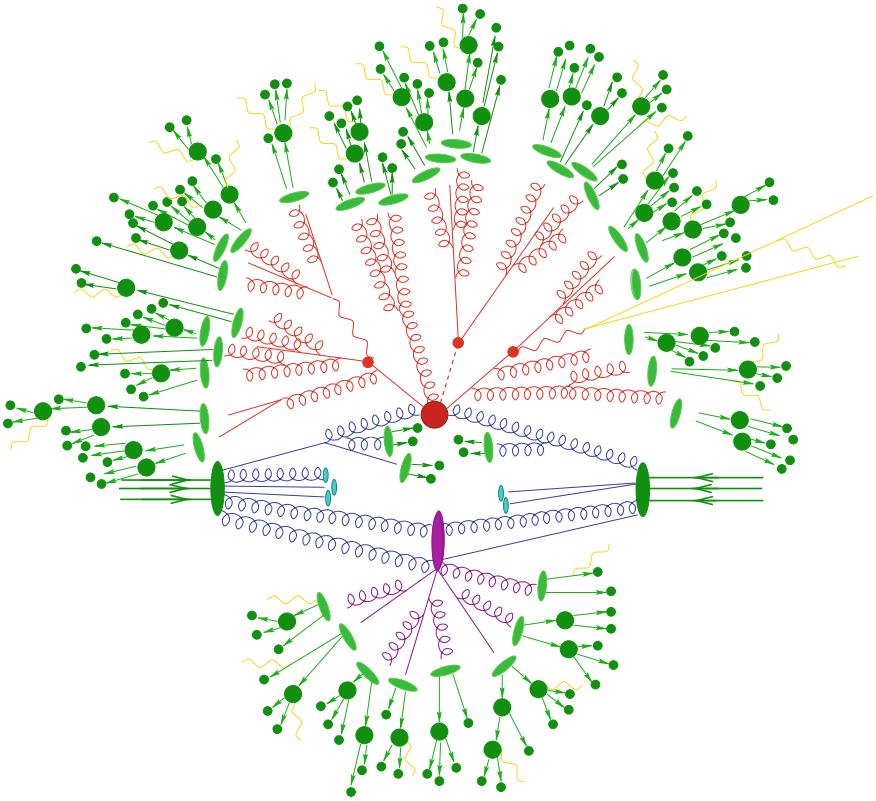

Fig. 2.3 Schematic diagram of a simulated ttH event, showing how factorisation allows the physics at different scales of momentum transfer Q to be treated independently [13]. At high-Q is the hard scatter (*red circle*). As the scale evolves down, partons are radiated in the initial state (*blue*) and final state (*red*). At low-Q, incoming partons are confined to the beam protons, while outgoing partons hadronise (*green blobs*). The underlying event comprises multiple partonic interactions (*purple blob*) and beam remnants (*blue blobs*). Photons and leptons (*yellow*) are also radiated

MSTW [11] and NNPDF [16]. PDFs differ because they are fit with different subsets of experimental data, massive quark treatments, parametrisation models and $\alpha_S(m_Z)$ values.

Final state radiation (FSR)

Soft and collinear radiation from outgoing partons is simulated by a universal parton shower, evolving the scale from the hard scatter to the hadronisation scale of $\sim$1 GeV. The successive emissions are ordered to avoid double-counting—typical order parameters are virtuality, transverse momentum and opening angle.

For the correct treatment of soft emissions, it is vital to preserve colour coherence. This is inherent in an angular ordered shower, but must be manually implemented otherwise. Alternatively, a *dipole shower* considers emissions from colour-connected pairs of partons, and is also inherently coherent.

Initial state radiation (ISR)
Soft and collinear radiation from incoming partons is similarly described by a parton shower. However, the small probability of evolving two partons with the kinematics required by the hard process necessitates a *backwards evolution*. Thus, the probability that a parton originated from one of higher momentum and lower scale is calculated, rather than an emission probability.

Hadronisation
The confinement of partons to hadrons is non-perturbative, and must be described by a hadronisation model. The *string model* stretches strings between colour partners. At some distance it becomes favourable to convert the potential energy to a $q\bar{q}$ pair, breaking the string. Once there is insufficient energy to create $q\bar{q}$ pairs, the hadrons 'freeze out'. The *cluster model* splits gluons into $q\bar{q}$ pairs, which group into colourless clusters with a mass spectrum predicted by QCD. These clusters then decay to the physical hadrons. Note that all hadronisation models require tuning to experimental data.

Hadron and τ decays
Many of the hadrons produced during hadronisation are unstable, and must be decayed to particles that are stable on a detector traversal timescale, while observing conservation laws and measured branching ratios. Similarly, the τ lepton must be decayed, hadronically or leptonically.

Multiple partonic interactions (MPI)
The *underlying event* (UE) is the additional soft hadronic activity caused by partons inactive in the hard scatter. It comprises the breakup of the beam remnants and *multiple partonic interactions* (MPI) between the protons. The size of the MPI activity is correlated to the scale of the hard scatter.

In order to calculate the number of additional interactions, the spatial distribution of partons within the proton must be modelled, the impact parameter of the pp collision must be known, and an IR cut-off must be imposed. This requires non-perturbative models that must be tuned to experimental data.

QED radiation
Electrically charged particles can emit photons at any stage of the event generation.

2.2.2 Summary of Event Generators

Three event generators are commonly used at the LHC, mainly differing in their choice of hadronisation and MPI models, and their parton shower order parameter. Efforts to rewrite the older Fortran-based programs in C++ have led to a generation of 'out-of-date' Fortran programs that are no longer actively developed. Even so, they are still in common usage, and so are included in the descriptions below.

Herwig

HERWIG (Fortran) [17] and HERWIG++ (C++) [18] both employ an angular ordered parton shower and a cluster hadronisation model. An MPI model is included in HERWIG++, but in HERWIG this was provided by JIMMY [19].

Pythia

PYTHIA 6 (Fortran) [20] and PYTHIA 8 (C++) [21] both use a string hadronisation model and an advanced MPI model. PYTHIA 8 uses a dipole shower ordered in transverse momentum, whereas PYTHIA 6 offers a choice of virtuality or transverse momentum ordered parton showers with colour coherence implemented manually.

Sherpa

SHERPA (C++) [22] uses a dipole shower ordered in transverse momentum, which is convenient for multi-leg merging (see Sect. 2.2.3). It uses a cluster hadronisation model and an MPI model similar to that of PYTHIA 8.

2.2.3 Multi-leg Merging

Although a parton shower excellently describes the emissions of large numbers of soft and collinear partons, it fails to accurately model hard and isolated emissions. It can be desirable to describe these using fixed order MEs, which are better suited to the task. In doing so, a couple of immediate issues arise. First, we require a smooth transition from the emissions of an ME to those of the parton shower. Second, each ME is inclusive, and attempting to combine MEs of differing multiplicity naturally leads to problems of double counting.

By using a merging prescription, such as the CKKW-L algorithm [23, 24] employed by SHERPA or the MLM algorithm [25] employed by ALPGEN [26] and MADGRAPH [27], it is possible to consistently combine LO matrix elements with differing multiplicities, whilst matching to the parton shower correctly. This does require the introduction of a merging scale though. This scale separates the ME and parton shower descriptions of the emissions, though the details of the separation depend upon the merging prescription.

2.2.4 NLO Matching

It is also possible to match an NLO ME to a parton shower, to improve the accuracy of both the normalisation and distribution of observables [28]. Such a calculation must include the LO, virtual-loop and real-emission diagrams, while mapping smoothly onto the parton shower for soft emissions. There are currently two valid matching prescriptions:

MC@NLO
Simply adding a parton shower to an NLO ME introduces double counting of emissions. The MC@NLO method compensates for this overlap through a correction to the NLO calculation. This correction renders the ME dependent upon the parton shower used in the MC event generator, and is also a source of negatively weighted events.

Originally implemented in the MC@NLO program for matching to HERWIG [29] and HERWIG++ [30], the method has now been automated within the aMC@NLO program [31] and extended for use with PYTHIA 6 and PYTHIA 8 [32]. It is now also included in SHERPA.

POWHEG
The POWHEG method requires the hardest emission to always be generated by the ME. It achieves the correct hard and soft behaviour by convolving the LO ME with a modified Sudakov factor, and then reweighting the differential cross section to the NLO result. Thus the ME is independent of the subsequent parton shower. However, if the parton shower is not transverse momentum ordered, it is necessary to use truncated and vetoed parton showers to correctly fill the phase space.

Originally implemented in POWHEGBOX [33–35], variants are now also included in HERWIG++ and SHERPA.

2.2.5 Additional Considerations

Detector simulation
In order to compare MC events to experimental events recorded at the LHC, it is vital to simulate how the outgoing particles interact with the detector. This is also necessary to calibrate the detector response and estimate efficiencies. GEANT4 [36, 37] is used to simulate the energy deposition of each particle during its trajectory through the ATLAS detector (see Chap. 3). Since long-lived particles will decay *en route*, particles with lifetime $c\tau > 10\,\text{mm}$ are decayed by GEANT4 rather than the MC generator. The majority of the simulation time is spent modelling the complex calorimeter geometry; in some cases

the simulation is performed by ATLFAST- II [38], which contains a simplified calorimeter simulation.

Digitisation converts the energy deposition into readout voltages and currents. Following this, the events can be treated like experimental collision events.

Pile-up simulation

As described in Chap. 3, each LHC bunch crossing can result in soft proton-proton interactions, known as *pile-up*, in addition to the hard process. This obscures the interesting physics and is important to model accurately.

In-time pile-up (same bunch crossing as the hard process) is modelled by overlaying simulated energy deposits from soft pp interactions generated with PYTHIA 8. The number of overlaid events depends upon the beam conditions (see Sect. 3.2).

Out-of-time pile-up (different bunch crossing to the hard process) affects detector sub-systems whose latency is longer than the bunch spacing. For such sub-systems, signals from out-of-time pile-up are overlaid with corresponding time shifts; again this depends on the beam conditions.

2.2.6 Parton Shower Tuning Study

When studying MC modelling uncertainties in the ggF process (see Sect. 5.2), a discrepancy was observed at high jet multiplicity between POWHEGBOX+PYTHIA 8 and POWHEGBOX+PYTHIA 6 (see the green and black lines in Fig. 2.4). It is also observed in other electroweak processes.

The hadronisation and UE models of standalone PYTHIA 8 have been tuned to ATLAS UE data with a variety of PDF sets (known as AU2 tunes) [39]. However, the parton shower was not tuned since the default settings successfully described experimental data.

When modelling ggF with POWHEGBOX, the AU2-CT10 tune was used in order to match the PDFs used in the matrix element calculation. Technically speaking, a dedicated POWHEGBOX+PYTHIA 8 tune should have been used, but this was unavailable. Unfortunately, a couple of issues had a negative impact on the NLO-PS matching. First, the parton shower evolves α_S at LO, whilst NLO PDFs were used in the shower. Second, there was a mismatch between the α_S used in POWHEGBOX, $\alpha_S(m_Z) = 0.118$, and the default value in the parton shower, $\alpha_S(m_Z) = 0.137$. The effect of these issues is shown in Fig. 2.4.

Identification of this poor matching has led to improvements in the latest round of MC tuning, where dedicated POWHEGBOX+PYTHIA 8 tunes are fit using an adjusted parton shower [40]. These shall be used in Run II.

2.3 Jet Algorithms

We have seen in Sect. 2.2 how coloured partons produced in a hard subprocess (in the ME) or radiated from the incoming partons (ISR) will each produce a shower of partons, which subsequently hadronise. By measuring the energy and direction of the resulting collimated *jet* of hadrons, it is possible to infer information about the original quark or gluon. This is very useful for probing the perturbative hard scatter, whilst remaining fairly insensitive to poorly understood hadronisation effects.

A *jet algorithm* defines how the large number of final state particle four-momenta are grouped into a small number of jet four-momenta. Such an algorithm should satisfy a number of criteria, the most important being infrared and collinear safety [41]. This requires that the jets are insensitive to additional soft or collinear emissions.

Multiple jet algorithms are implemented in the FastJet software library [42]. In particular, *sequential recombination algorithms* are popular at the LHC, which iteratively combine the closest pair of particles according to some distance measure d_{ij}.

Consider an algorithm where all the inter-particle distances d_{ij} and particle-beam distances $d_{i\mathrm{B}}$ are calculated. If the minimum of these is a d_{ij} rather than a $d_{i\mathrm{B}}$, then particles i and j are combined into single new particle. If the minimum is a $d_{i\mathrm{B}}$, then particle i is declared a jet and removed from the list of particles. Then the algorithm restarts. We define the distances

$$d_{ij} = \min\left(p_{\mathrm{T}i}^{2m}, p_{\mathrm{T}j}^{2m}\right)\frac{\Delta R_{ij}^2}{R^2}, \qquad \Delta R_{ij}^2 = \left(y_i - y_j\right)^2 + \left(\phi_i - \phi_j\right)^2 \tag{2.8}$$

$$d_{i\mathrm{B}} = p_{\mathrm{T}i}^{2m} \tag{2.9}$$

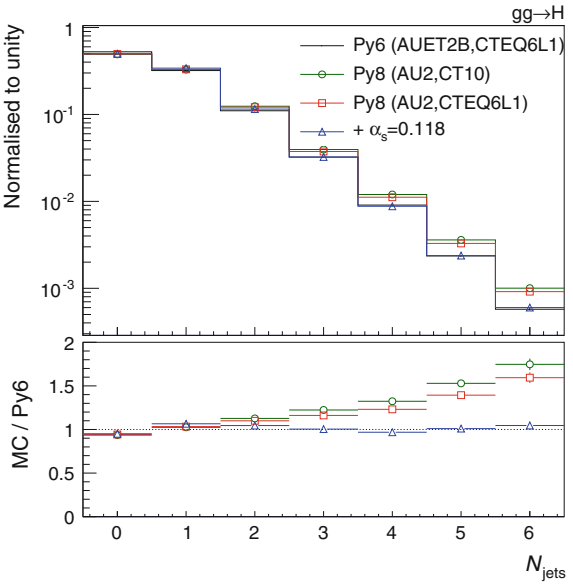

Fig. 2.4 Jet multiplicity produced by PowhegBox+Pythia 8 with a selection of shower tunes. The *green circles* correspond to the tune used in the analysis. The *red squares* change the parton shower PDFs from CT10 to CTEQ6L1. The *blue triangles* additionally change the parton shower $\alpha_{\mathrm{S}}(m_Z)$ from 0.137 to 0.118 (as used in PowhegBox). PowhegBox+Pythia 6 is shown in *black* for reference, and is in good agreement with PowhegBox+Herwig (not shown)

where $p_{\mathrm{T}i}$, y_i and ϕ_i are the transverse momentum, rapidity and azimuthal angle of particle i with respect to the beam axis, respectively. R and m are parameters of the algorithm, with R effectively determining the size of the jet.

With $m = 1$, known as the k_{T} algorithm, combinations between soft particles are favoured. This follows the evolution of QCD, but leads to rather irregular jet shapes.

With $m = -1$, known as the anti-k_{T} algorithm [43], combinations between hard particles are favoured. This means the jets grow outwards from a hard 'seed', ultimately producing more circular jets. However, the jet substructure can no longer be used to infer details of the jet evolution history. The jets used in this thesis were anti-k_{T} jets with $R = 0.4$, and their reconstruction shall be described in detail in Sect. 4.2.5.

References

1. R.K. Ellis, W.J. Stirling, B.R. Webber, *QCD and Collider Physics* (Cambridge University Press, Cambridge, 1996)
2. I.J.R. Aitchison, A.J.G. Hey, *Gauge Theories in Particle Physics*, 3rd edn. (Taylor and Francis, Abingdon, 2003)
3. K.G. Wilson, Confinement of quarks. Phys. Rev. D **10**, 2445 (1974)
4. D.J. Gross, F. Wilczek, Ultraviolet behavior of non-Abelian Gauge theories. Phys. Rev. Lett. **30**, 1343 (1973)
5. H.D. Politzer, Reliable perturbative results for strong interactions? Phys. Rev. Lett. **30**, 1346 (1973)
6. Particle Data Group, Review of particle physics. Phys. Rev. D **86**, 010001 (2012), and 2013 partial update for the 2014 ed
7. J.C. Collins, D.E. Soper, Parton distribution and decay functions. Nucl. Phys. B **194**, 445 (1982)
8. V.N. Gribov, L.N. Lipatov, Deep inelastic *ep* scattering in perturbation theory. Sov. J. Nucl. Phys. **15**, 438 (1972)
9. G. Altarelli, G. Parisi, Asymptotic freedom in parton language. Nucl. Phys. B **126**, 298 (1977)
10. Y. L. Dokshitser, Calculation of structure functions of deep inelastic scattering and e^+e^- annihilation by perturbative theory in quantum chromodynamics. Sov. Phys.-JETP **46**, 641 (1977)
11. A.D. Martin, W.J. Stirling, R.S. Thorne, G. Watt, Parton distributions for the LHC. Eur. Phys. J. C **63**, 189 (2009), arXiv:0901.0002 [hep-ph]
12. A. Buckley et al., General-purpose event generators for LHC physics. Phys. Rep. **504**, 145 (2011), arXiv:1101.2599 [hep-ph]
13. S. Höche, Matching to matrix elements, in MCnet-LPCC Summer School on Monte Carlo Event Generators for LHC, Geneva (2012)
14. M.R. Whalley, D. Bourilkov, R.C. Group, The Les Houches accord PDFs (LHAPDF) and LHAGLUE, in HERA and the LHC, Hamburg (2005), arXiv:hep-ph/0508110
15. H.-L. Lai et al., New parton distributions for collider physics. Phys. Rev. D **82**, 074024 (2010), arXiv:1007.2241 [hep-ph]
16. R.D. Ball et al., Parton distributions with LHC data. Nucl. Phys. B **867**, 244 (2013), arXiv:1207.1303 [hep-ph]
17. G. Corcella et al., HERWIG 6: an event generator for hadron emission reactions with interfering gluons (including supersymmetric processes). JHEP **0101**, 010 (2001), arXiv:hep-ph/0210213
18. M. Bähr et al., Herwig++ physics and manual. Eur. Phys. J. C **58**, 639 (2008), arXiv:0803.0883 [hep-ph]

19. J.M. Butterworth, J.R. Forshaw, M.H. Seymour, Multiparton interactions in photoproduction at HERA. Z. Phys. C **72**, 637 (1996), arXiv:hep-ph/9601371
20. T. Sjöstrand, S. Mrenna, P. Skands, PYTHIA 6.4 physics and manual. JHEP **0605**, 026 (2006), arXiv:hep-ph/0603175
21. T. Sjöstrand, S. Mrenna, P. Skands, A brief introduction to PYTHIA 8.1. Comput. Phys. Commun. **178**, 852 (2008), arXiv:0710.3820[hep-ph]
22. T. Gleisberg et al., Event generation with SHERPA 1.1. JHEP **0902**, 007 (2009), arXiv:0811.4622 [hep-ph]
23. S. Catani, F. Krauss, R. Kuhn, B.R. Webber, QCD matrix elements + parton showers. JHEP **0111**, 063 (2001), arXiv:hep-ph/0109231
24. L. Lonnblad, Correcting the color-dipole cascade model with fixed order matrix elements. JHEP **0205**, 046 (2002), arXiv:hep-ph/0112284
25. S. Hoeche et al., Matching parton showers and matrix elements (2006), arXiv:hep-ph/0602031
26. M.L. Mangano, M. Moretti, F. Piccinini, R. Pittau, A.D. Polosa, ALPGEN, a generator for hard multiparton processes in hadronic collisions. JHEP **0307**, 001 (2003), arXiv:hep-ph/0206293
27. J. Alwall, M. Herquet, F. Maltoni, O. Mattelaer, T. Stelzer, MadGraph 5: going beyond. JHEP **1106**, 128 (2011), arXiv:1106.0522 [hep-ph]
28. P. Nason, B. Webber, Next-to-leading-order event generators. Ann. Rev. Nucl. Part. Sci. **62**, 187 (2012), arXiv:1202.1251 [hep-ph]
29. S. Frixione, B.R. Webber, Matching NLO QCD computations and parton shower simulations. JHEP **0206**, 029 (2002), arXiv:hep-ph/0204244
30. S. Frixione, F. Stoeckli, P. Torrielli, B.R. Webber, NLO QCD corrections in Herwig++ with MC@NLO. JHEP **1101**, 053 (2011), arXiv:1010.0568 [hep-ph]
31. V. Hirschi et al., Automation of one-loop QCD corrections. JHEP **1105**, 044 (2011), arXiv:1103.0621 [hep-ph]
32. P. Torrielli, S. Frixione, Matching NLO QCD computations with PYTHIA using MC@NLO. JHEP **1004**, 110 (2010), arXiv:1002.4293 [hep-ph]
33. P. Nason, A new method for combining NLO QCD with shower Monte Carlo algorithms. JHEP **0411**, 040 (2004), arXiv:hep-ph/0409146
34. S. Frixione, P. Nason, C. Oleari, Matching NLO QCD computations with parton shower simulations: the POWHEG method. JHEP **0711**, 070 (2007), arXiv:0709.2092 [hep-ph]
35. S. Alioli, P. Nason, C. Oleari, E. Re, A general framework for implementing NLO calculations in shower Monte Carlo programs: the POWHEG BOX. JHEP **1006**, 043 (2010), arXiv:1002.2581 [hep-ph]
36. S. Agostinelli et al., Geant4—a simulation toolkit. Nucl. Instrum. Methods **A506**, 250 (2003)
37. ATLAS Collaboration, The ATLAS simulation infrastructure, Eur. Phys. J. C **70**, 823 (2010), arXiv:1005.4568[physics.ins-det]
38. ATLAS Collaboration, The simulation principle and performance of the ATLAS fast calorimeter simulation FastCaloSim, ATL-PHYS-PUB-2010-013 (2010)
39. ATLAS Collaboration, Summary of ATLAS Pythia 8 tunes. ATL-PHYS-PUB-2012-003 (2012)
40. ATLAS Collaboration, Example ATLAS tunes of Pythia8, Pythia6 and Powheg to an observable sensitive to Z boson transverse momentum. ATL-PHYS-PUB-2013-017 (2013)
41. G.P. Salam, Towards jetography. Eur. Phys. J. C **67**, 637 (2010), arXiv:0906.1833 [hep-ph]
42. M. Cacciari, G.P. Salam, G. Soyez, FastJet user manual. Eur. Phys. J. C **72**, 1896 (2012), arXiv:1111.6097 [hep-ph]
43. M. Cacciari, G.P. Salam, G. Soyez, The anti-k_t jet clustering algorithm. JHEP **0804**, 063 (2008), arXiv:0802.1189 [hep-ph]

http://www.springer.com/978-3-319-19988-7

Discovery and Measurement of the Higgs Boson in the WW Decay Channel

Hall, D.

2015, XX, 160 p. 75 illus., 57 illus. in color., Hardcover
ISBN: 978-3-319-19988-7